OAK RIDGE
NATIONAL LABORATORY
MANAGED BY UT-BATTELLE
FOR THE DEPARTMENT OF ENERGY

ORNL/TM-2013/172

Modeling the Effect of High Background Mitigation Techniques on Radiation Portal Monitors

May 2013

Prepared by

Tyler Guzzardo
Alexander Solodov
Jake Livesay
Ian Gross

UT-BATTELLE
ORNL-27 (4-00)

ORNL/TM-2013/172

Nuclear Security and Isotope Technology Division

Modeling the Effect of High Background Mitigation Techniques on Radiation Portal Monitors

Tyler Guzzardo
Alexander Solodov*
Jake Livesay**
Ian Gross

*Khalifa University of Science, Technology & Research
**Mason Livesay Scientific

Date Published: May 2013

Prepared by
OAK RIDGE NATIONAL LABORATORY
Oak Ridge, Tennessee 37831-6283
managed by
UT-BATTELLE, LLC
for the
U.S. DEPARTMENT OF ENERGY
under contract DE-AC05-00OR22725

CONTENTS

Page

ABBREVIATED TERMS

Bq	Becquerel
Ci	Curie
cm	centimeter
ISOCS	In Situ Object Counting System
keV	kilo electron volts
m	meter
MCA	multichannel analyzer
MCNP	Monte Carlo N-Particle
MeV	mega electron volts
NAA	neutron activation analysis
ORNL	Oak Ridge National Laboratory
PVT	polyvinyl toluene
RPM	radiation portal monitor
SLD	Second Line of Defense
SNM	special nuclear material

LIST OF TABLES

LIST OF FIGURES

EXECUTIVE SUMMARY

The Oak Ridge National Laboratory (ORNL) has been tasked by the United States National Nuclear Security Administration's Second Line of Defense (SLD) program with determining a viable method for mitigating high background radiation levels in radiation portal monitors (RPM). High background radiation levels adversely affect the ability of RPMs to detect small sources of radiation. For this reason, it is desirable to install RPMs in low background environments where a low false alarm rate can be achieved and small deviations in detector signals are able to trigger alarms. To investigate the mitigation of high background levels, a test bed was established at ORNL capable of reproducing many factors that contribute to radiation background levels. The controlled environment of the test bed allows the isolation of a variety of factors that influence background and are difficult to accurately characterize in the field. In this work, the test bed is used to characterize numerous RPM configurations encountered in the field and provide a benchmark for modeling RPM background levels. Accurately modeling the background measured by a RPM allows future background remediation techniques to first be modeled to test their validity before being installed in the field. The utilization of these tools can yield a cost savings to the program by minimizing costly field installations and understanding the outcome of remediation techniques prior to widespread implementation.

1. INTRODUCTION

The radiation portal monitor (RPM) test bed (Figure 1) at Oak Ridge National Laboratory (ORNL) has been used to study possible background remediation techniques through the measurement and modeling of different RPM configurations. A variety of RPM configurations were measured in different background environments by a TSA Systems VM-250AGN[1] vehicle monitor to provide a realistic benchmark capable of verifying the accuracy of radiation transport computer models. An accurate RPM model allows the impact of background remediation techniques to be calculated before configuration changes are made in the field. Understanding how background radiation levels contribute to RPM count rates can provide a cost savings to the program by preventing the installation of background remediation techniques that do not lower the RPM count rate as expected.

Figure 1. ORNL RPM test bed.

2. ORNL RPM TEST BED

2.1 Capabilities

The test bed has the unique capability of altering the background environment experienced by the RPM through the movement of concrete slabs placed between the RPM pillars (Figure 2). The slabs contain varying concentrations of granite aggregate that produce a different activity level for each slab. Three concrete slabs, referred to as Slabs G, F, and L, are available for measurement in addition to the natural background provided by the asphalt present at the site. The concrete slabs measure 396.1 cm × 457.0 cm × 30.5 cm and were constructed to fit between vehicle monitors of typical spacing.

In addition to changing the source of the background activity, radiation from the source can be attenuated by different shielding configurations at the test bed. Collimators (Figure 3) and shadow shields (Figure 4) are available for testing their ability to reduce the background level measured by the RPM. The set of four 1-cm-thick TSA Systems lead collimators measure 79.7 cm × 18.0 cm × 18.7 cm. The custom-built set of four 2.54-cm-thick iron shadow shields, each measuring 121.5 cm × 304.5 cm × 2.5 cm, can be attached to each pillar to shield radiation originating behind the RPM. Changing the shielding configuration requires the assistance of a rigging crew capable of lifting the shadow shields and lowering the pillars to install collimators (Figure 5).

Figure 2. Concrete slab between RPM pillars.

Figure 3. TSA Systems lead collimators.

Figure 4. Custom-built shadow shields shown on one RPM pillar.

Figure 5. Rigging crew lowering the RPM pillar for collimator installation.

2.2 Calibration

Before any measurements were conducted at the test site, the RPM was calibrated and the detector efficiencies were calculated. This ensured that the correct operational settings were used so the RPM at the test bed could be compared to RPMs deployed across the Second Line of Defense (SLD) program. The lower and upper level discriminators were set to equate to a region of interest of approximately 25–40 keV. The gamma detectors were calibrated with a multichannel analyzer (MCA) by following the "Multichannel Analyzer Alignment Procedure for TSA Radiation Portal Monitors."[2] Additional details regarding the calibration are in Section A.1 of Appendix A. The efficiencies of the gamma detectors were calculated by following the "Second Line of Defense Functional Compliance Test Procedure for TSA Radiation Portal Monitors."[3] As shown in Table 1, expected values were calculated for all the detector efficiencies. Additional details regarding the efficiency calculation are in Section A.1 of Appendix A.

Table 1. Gamma detector efficiencies

Detector number	Efficiency (%)
D1 (Master Lower)	26
D2 (Master Upper)	25
D3 (Slave Lower)	33
D4 (Slave Upper)	34

3. DATA ACQUISTION

3.1 RPM Field Data

Data were collected at the RPM test bed with the TSA Systems VM-250AGN vehicle monitor to provide a reliable base case that computer models could be benchmarked against. Four RPM configurations were used in three different background environments to obtain a set of 12 measurement points for verifying computer models. The different configurations include the independent concrete slab, the slab with

shadow shields, the slab with collimators, and the slab with shadow shields and collimators. Each configuration has a corresponding configuration number to aid plotting of data (Table 2).

Table 2. RPM configuration elements

Configuration elements	Configuration number
Concrete slab only	1
Slab and shadow shields	2
Slab and collimation	3
Slab, shadow shields, and collimation	4

Data was acquired from each RPM configuration for multiple days to obtain an accurate measurement of the steady-state RPM background level. From the days of data recorded, a segment of the data stream was chosen for analysis that was not influenced by external factors such as rainstorms[4] or irregular detector noise.[*] The average detector count rate was then calculated from the chosen segment of data. To determine if the RPM provided reliable test results, graphical data was examined throughout the test campaign for irregular data patterns and control data was recorded before and after testing with only the asphalt source present. Shown in Table 3, the selected RPM data can be expected to be accurate to within approximately 5% of the measured value.

Table 3. Control data for RPM with only asphalt source present

	D1	D2	D3	D4	Total
Count rate before testing (counts/sec)	116 ± 0.12	123 ± 0.12	132 ± 0.12	155 ± 0.13	526 ± 0.25
Count rate after testing (counts/sec)	111 ± 0.08	112 ± 0.08	124 ± 0.08	150 ± 0.09	498 ± 0.17
Percent change (%)	4 ± 0.12	9 ± 0.12	6 ± 0.11	3 ± 0.11	5 ± 0.06

Figures 6–8 and Tables 4–6 contain the data recorded from the RPM for all configurations. The field data has been corrected for efficiency, making the plotted data more representative of the implemented configuration than the efficiency of the detectors; all detectors are normalized to an efficiency of 25%. Figures 6–8 show Slab G contains the highest activity, Slab L contains the second highest, and Slab F contains the lowest activity, respectively. As expected, the shadow shields provide a relatively small reduction in background because they are limited to attenuating gammas originating behind the RPM pillars. A large reduction in background was experienced from the lead collimators, and a combination of the shadow shields and collimators provided the greatest reduction in background. Uncertainties from counting statistics for the RPM count rates were propagated and are shown in Tables 4–6, but are not shown in Figures 6–8 due to their low magnitude.

[*] Section A.3 of Appendix A graphically shows how the RPM data was selected.

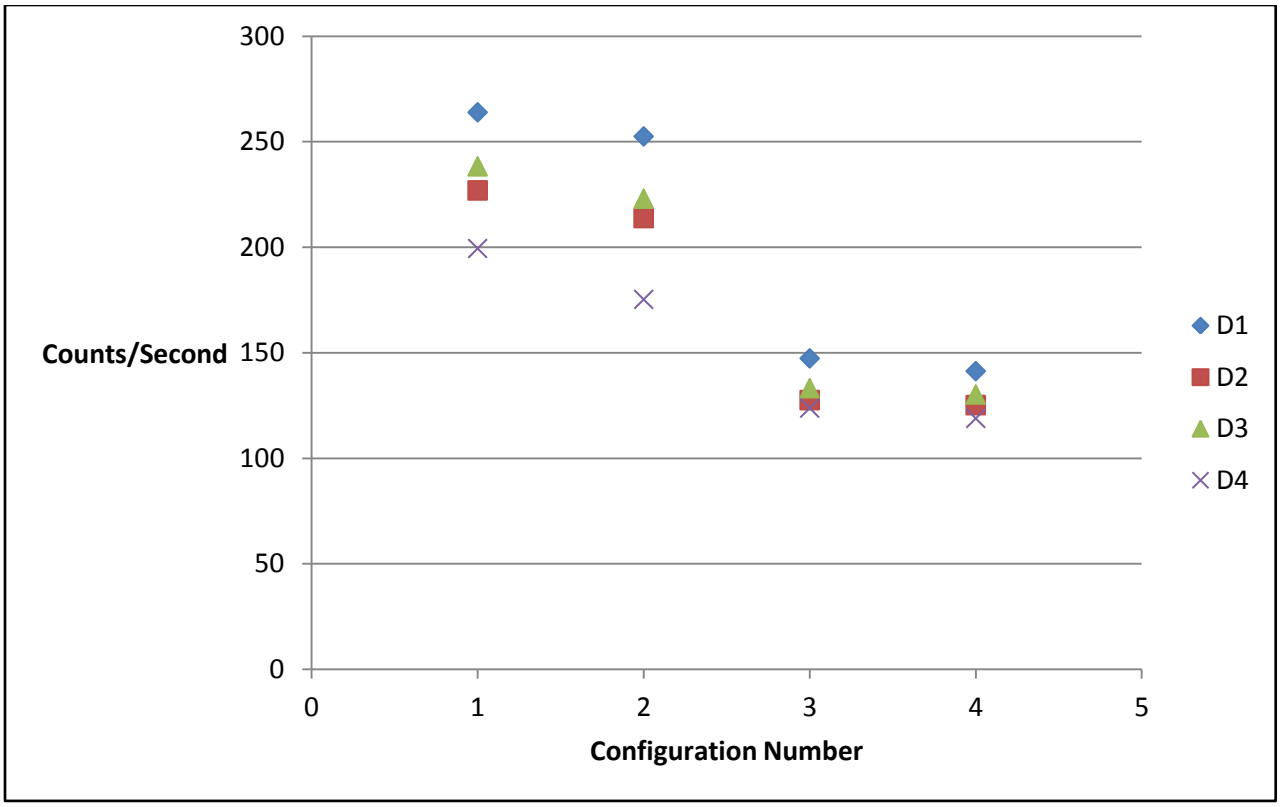

Figure 6. A plot of Slab G RPM field data.

Table 4. Slab G RPM field data

Configuration Number	Detector Number	Count Rate (Counts/second)
1 (Slab)	D1	264 ± 0.08
	D2	227 ± 0.08
	D3	238 ± 0.07
	D4	199 ± 0.06
2 (Shadow shields)	D1	253 ± 0.19
	D2	214 ± 0.18
	D3	223 ± 0.16
	D4	175 ± 0.14
3 (Collimators)	D1	147 ± 0.10
	D2	128 ± 0.10
	D3	133 ± 0.09
	D4	124 ± 0.08
4 (Collimators and shadow shields)	D1	141 ± 0.07
	D2	125 ± 0.07
	D3	130 ± 0.06
	D4	119 ± 0.06

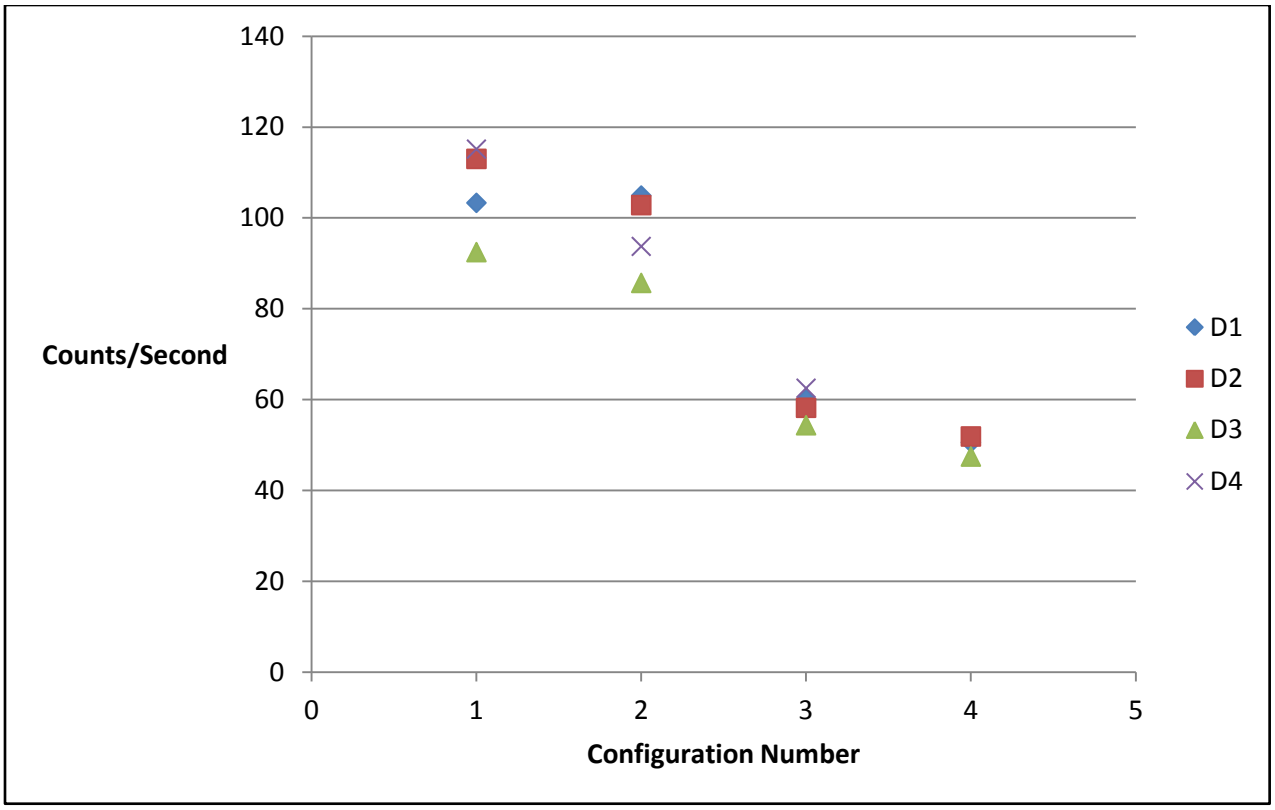

Figure 7. A plot of Slab F RPM field data.

Table 5. Slab F RPM field data

Configuration Number	Detector Number	Count Rate (Counts/second)
1 (Slab)	D1	103 ± 0.08
	D2	113 ± 0.08
	D3	92 ± 0.06
	D4	115 ± 0.07
2 (Shadow shields)	D1	105 ± 0.05
	D2	103 ± 0.05
	D3	86 ± 0.04
	D4	94 ± 0.04
3 (Collimators)	D1	60 ± 0.07
	D2	58 ± 0.07
	D3	54 ± 0.06
	D4	63 ± 0.06
4 (Collimators and shadow shields)	D1	51 ± 0.05
	D2	52 ± 0.05
	D3	47 ± 0.05
	D4	53 ± 0.05

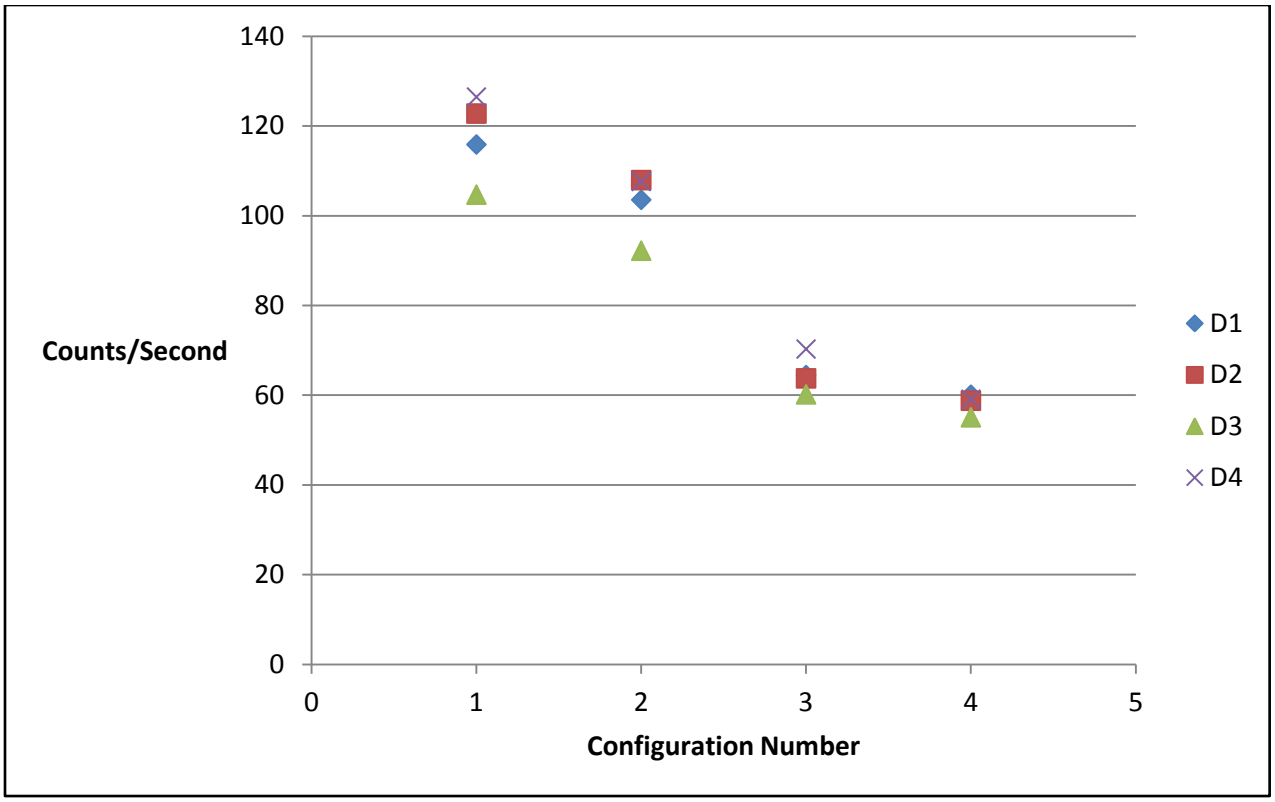

Figure 8. A plot of Slab L RPM field data.

Table 6. Slab L RPM field data

Configuration Number	Detector Number	Count Rate (Counts/second)
1 (Slab)	D1	116 ± 0.07
	D2	123 ± 0.08
	D3	105 ± 0.06
	D4	126 ± 0.07
2 (Shadow shields)	D1	104 ± 0.09
	D2	108 ± 0.09
	D3	92 ± 0.07
	D4	108 ± 0.08
3 (Collimators)	D1	64 ± 0.012
	D2	64 ± 0.012
	D3	60 ± 0.10
	D4	70 ± 0.11
4 (Collimators and shadow shields)	D1	60 ± 0.07
	D2	59 ± 0.07
	D3	55 ± 0.06
	D4	59 ± 0.06

3.2 ISOCS Field Data

To develop a model of the RPM capable of reproducing the recorded RPM field data, accurate source terms were required for the asphalt and concrete slabs. Spectra were recorded from the asphalt and the concrete with a high-purity germanium detector to determine the radioactive constituents of the sources. In a previous study conducted by Ryan,[5] spectra of concrete core samples were recorded, and in the present work, the asphalt was measured (Figure 9) to account for its contribution to the background radiation level. The spectra were then analyzed with the In Situ Object Counting System[6] (ISOCS) software to create an efficiency calibration (Figure 10). The efficiency calibration allowed specific activities to be calculated for the different isotopes present in the asphalt and concrete. The gamma energies and branching ratios used in the analysis are shown in Table 7. Most of the activity resulted from primordial nuclides present in the decay chains of K-40, Th-232, and U-238. However, a small amount of Cs-137 was detected in the asphalt at the test bed. Ultimately, the data utilized from the ISOCS analysis includes the specific activities of each background source (Table 8) and the total activities corrected for mass and isotopic branching ratio (Table 9). The source terms produced for each background source are shown in Section A.2 of Appendix A.

Figure 9. ISOCS measurement of asphalt at test bed.

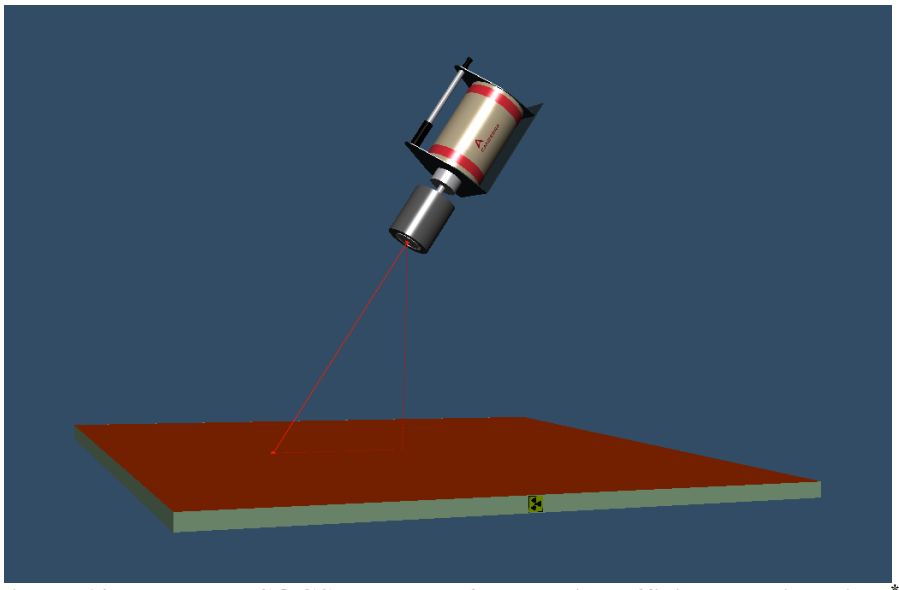

Figure 10. Example ISOCS geometry for creating efficiency calibration.[*]

Table 7. Gamma properties used for source term analysis

Decay Chain	Isotope	Gamma Energy (MeV)	Gamma Yield
K-40	K-40	1.46081	0.1067
Cs-137	Cs-137	0.66166	0.9472
Th-232	Tl-208	0.27736	0.0227
		0.58319	0.3037
		0.86056	0.0446
		2.61453	0.3564
	Bi-212	0.72733	0.1027
	Pb-212	0.23863	0.4330
		0.30009	0.0328
	Ac-228	0.12907	0.0242
		0.27024	0.0346
		0.32803	0.0295
		0.33832	0.1127
		0.40946	0.0192
		0.46300	0.0440
		0.79495	0.0425
		0.91120	0.2580
		0.96477	0.0499
		0.96897	0.1580

[*] The ISOCS geometry shown in Figure 10 is abridged from the actual geometry used for this work for illustrative purposes.

Table 8. (continued)

Decay Chain	Isotope	Gamma Energy (MeV)	Gamma Yield
U-238	Bi-214	0.60931	0.4610
		0.76836	0.0494
		0.93406	0.0303
		1.12039	0.1510
		1.23811	0.0579
		1.37767	0.0400
		1.76449	0.1540
		2.20421	0.0508
	Pb-214	0.24200	0.0743
		0.29522	0.1930
		0.35193	0.3760
	Ra-226	0.18621	0.0359
	Th-234	0.06329	0.0480
		0.09260	0.0557

Table 9. Asphalt and concrete specific activity

	Specific Activity (Bq/kg)			
Decay Chain	Asphalt	Slab G	Slab F	Slab L
K-40	260.5 ± 11.3	696.1 ± 30.1	42.3 ± 4.7	170.3 ± 8.8
Th-232	5.8 ± 0.2	80.2 ± 1.6	5.0 ± 0.4	9.6 ± 0.5
U-238	10.7 ± 0.3	112.6 ± 5.5	23.4 ± 2.3	28.6 ± 2.6
Cs-137	2.9 ± 0.2	-	-	-

Table 10. Total background activities corrected for branching ratio and mass

Source	Activity (Bq)
Asphalt	3.80×10^{7}
Slab G	4.44×10^{6}
Slab F	4.31×10^{5}
Slab L	7.68×10^{5}

4. MONTE CARLO ANALYSIS

4.1 Model Design

The radiation transport computer model created in MCNP[7] (Figures 11 and 12) was designed through numerous iterations to ensure it represented the RPM at the test bed as accurately as possible. In addition to the present work, the input decks have been modified by Solodov, Ryan, and Fitzmaurice.[8] Ultimately, a combination of a large atmosphere, concrete layered for variance reduction, and separate asphalt and concrete input decks allowed for a sufficiently realistic model.

The spherical atmosphere used in the model had a 1300 m radius that allowed sufficient scattering of the gammas emitted from the 74 m × 74 m asphalt. The size of the atmosphere to use in the model was determined by varying the atmosphere radius and tracking the change in the detector response. Due to the gammas ability to easily scatter through the atmosphere and still be detected by the RPM, it was determined a 1300 m radius atmosphere was required for the model to produce an unbiased result.

The concrete slab defined in the model was split into three different layers to utilize a common variance reduction technique, geometry splitting.[9] Due to the large thickness of the concrete, many of the source particles tracked by MCNP would not penetrate the concrete and ultimately not be detected. Executing an analog model in this manner would require excessive computational time to obtain a low relative error. Alternatively, geometry splitting was used in the different concrete layers to allow increased tracking of particles of interest while still ensuring undistorted results.

Separate input decks were created for calculating the detector response from radiation emitted from the asphalt and the concrete. Due to the large volume of asphalt used in the model, a disproportionate amount of activity was present in the asphalt. Thus if two source cards were used in one input deck, the source card for the concrete would be sampled so few times that a prohibitively large number of source particles would be required. Separating the source cards in different input decks allowed adequate sampling from both sources. The activities of each source calculated from ISOCS allowed the detection probabilities from the model to be corrected and combined.

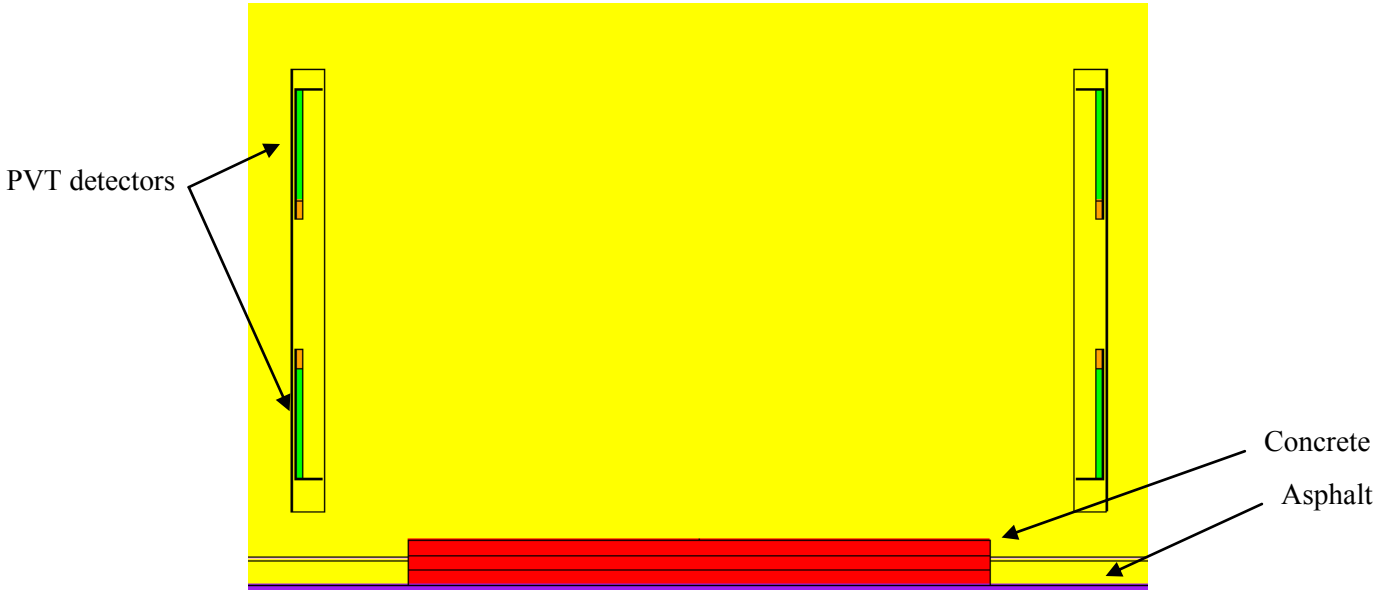

Figure 11. Cross-sectional view of RPM in model.

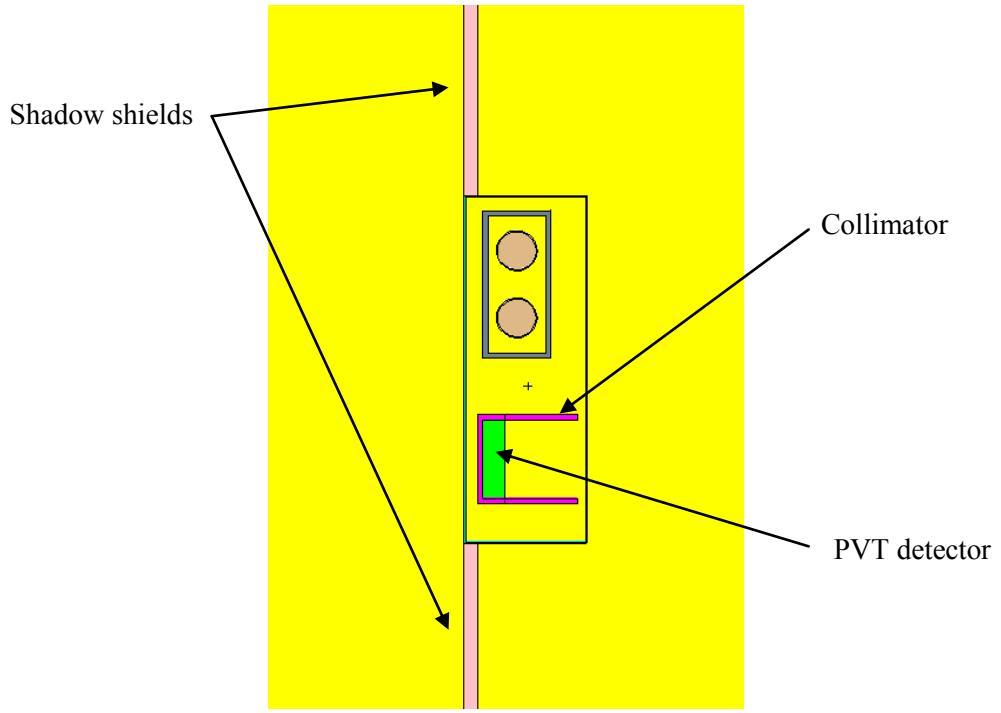

Figure 12. Detailed cross-sectional view of collimator and shadow shields in model.

4.2 Material Definitions

The material definitions of concrete used in the model were calculated by neutron activation analysis (NAA) in previous work conducted by Ryan.[5] Neutron activation analysis is a complex method of determining material properties by irradiating a sample with neutrons and measuring the decay of the product nuclides. A high flux of neutrons is required for the analysis and is normally provided by a nuclear reactor. This type of analysis and other destructive techniques that require acquisition of a material sample are not suitable for routine field use. However, the material properties of concrete and asphalt are largely dependent on the type of aggregate used. If the aggregate material can be determined, an accurate material definition can be obtained from material data sheets developed for radiation transport modeling.[10] The attenuation coefficients for the energies of interest are the most important characteristic of the material definition for modeling and can be more easily estimated than the exact isotopic composition. Since the material definitions in the model do not contribute to the radiation source term and large differences in isotopic composition are not expected for concrete and asphalt, an estimate of the RPM detector response can still be calculated without measuring precise material compositions.

5. RESULTS

To compare the results of the model with the RPM benchmark values, the fraction of background measured by the RPM was calculated after each configuration change (Figures 13–15). Measurements with only the concrete slab in place were used as a base case from which to compare all the remediation techniques. For instance, the fraction of background measured by Configuration 3 was calculated by dividing the count rate from slab G with collimators by the count rate from slab G only. In all cases, the model proved capable of calculating the expected reduction in background to within 10%. The uncertainties listed in Tables 10–12 are limited to counting statistics and are not representative of total measurement uncertainty.

In general, the model replicated the measured RPM data and calculated the expected results. The model calculated the largest reduction in background from Configuration 4 with both the collimators and the shadow shields installed. The smallest reduction in background was produced by Configuration 2 with only the shadow shields installed. The data illustrates broad trends in the reduction of background caused by a remediation technique are easily determined by the model. However, differences between the model and the RPM data for a given configuration show sources of error are present that are not attributed to counting statistics.

The model did not calculate a large enough reduction in background for Configuration 2 from Slabs G and L. This result was caused by the model calculating different probabilities of interaction from the slab and asphalt input decks. The slab input deck for Configuration 2 produced an interaction probability greater than the base case due to gammas from the concrete scattering off the shadow shields and into the detectors. This only amounted to an approximately 1% increase in count rate due to the relatively low probability of this scattering event. The asphalt input deck for Configuration 2 resulted in a significantly lower interaction probability than the base case due to the attenuation of gammas in the shadow shield that originated in the asphalt outside of the RPM pillars. However, when the interaction probabilities were corrected for specific activity, the majority of the count rate resulted from the slab input deck, therefore giving less weight to the lower interaction probability from the asphalt input deck. These differences show opportunities for improvement in the model, but are not of great concern since the majority of the results are within the expected accuracy of 5% (Table 3).

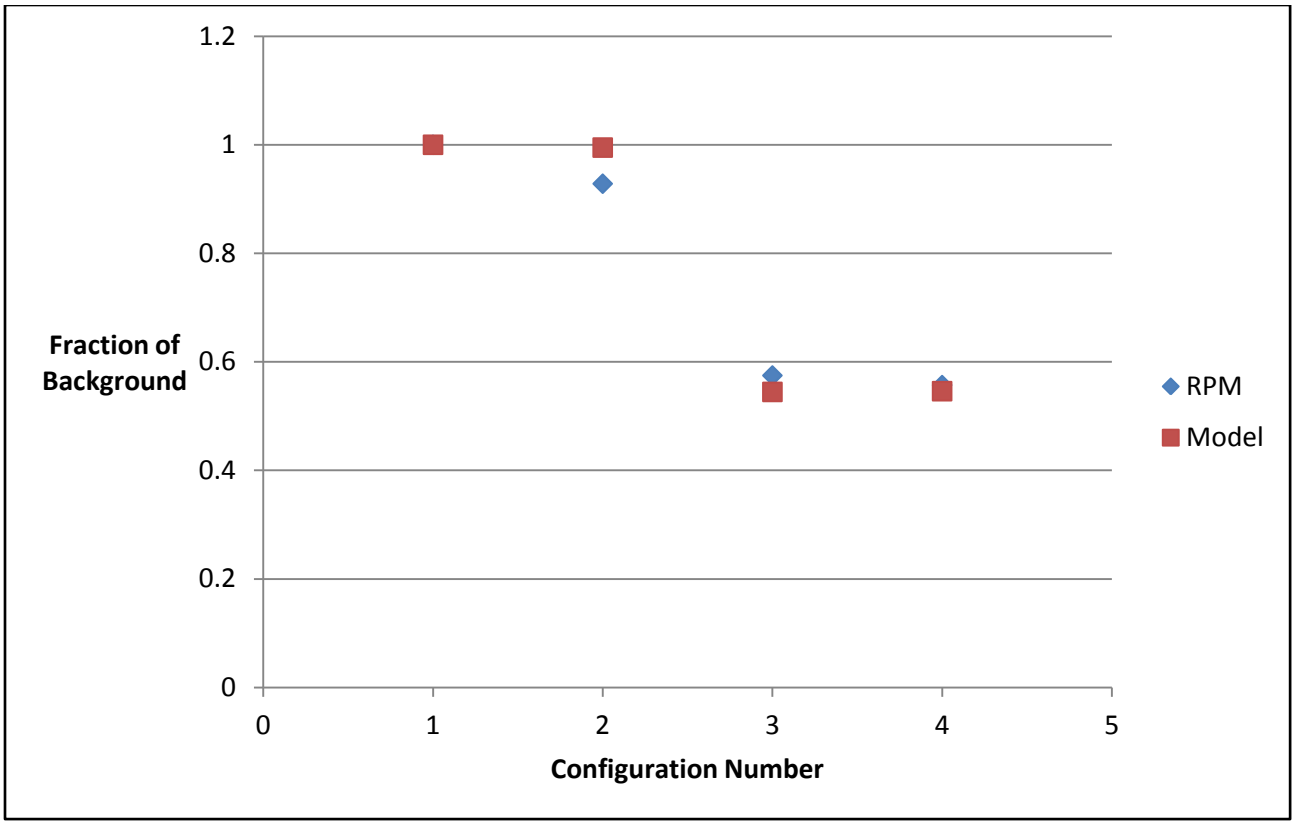

Figure 13. A plot of the fraction of background calculated from Slab G RPM and model data.

Table 11. Slab G RPM and model background comparison

	Fraction of Background	
Configuration Number	RPM	Model
1	1	1
2	0.93 ± 0.0004	0.99 ± 0.01
3	0.57 ± 0.0002	0.54 ± 0.01
4	0.56 ± 0.0002	0.55 ± 0.01

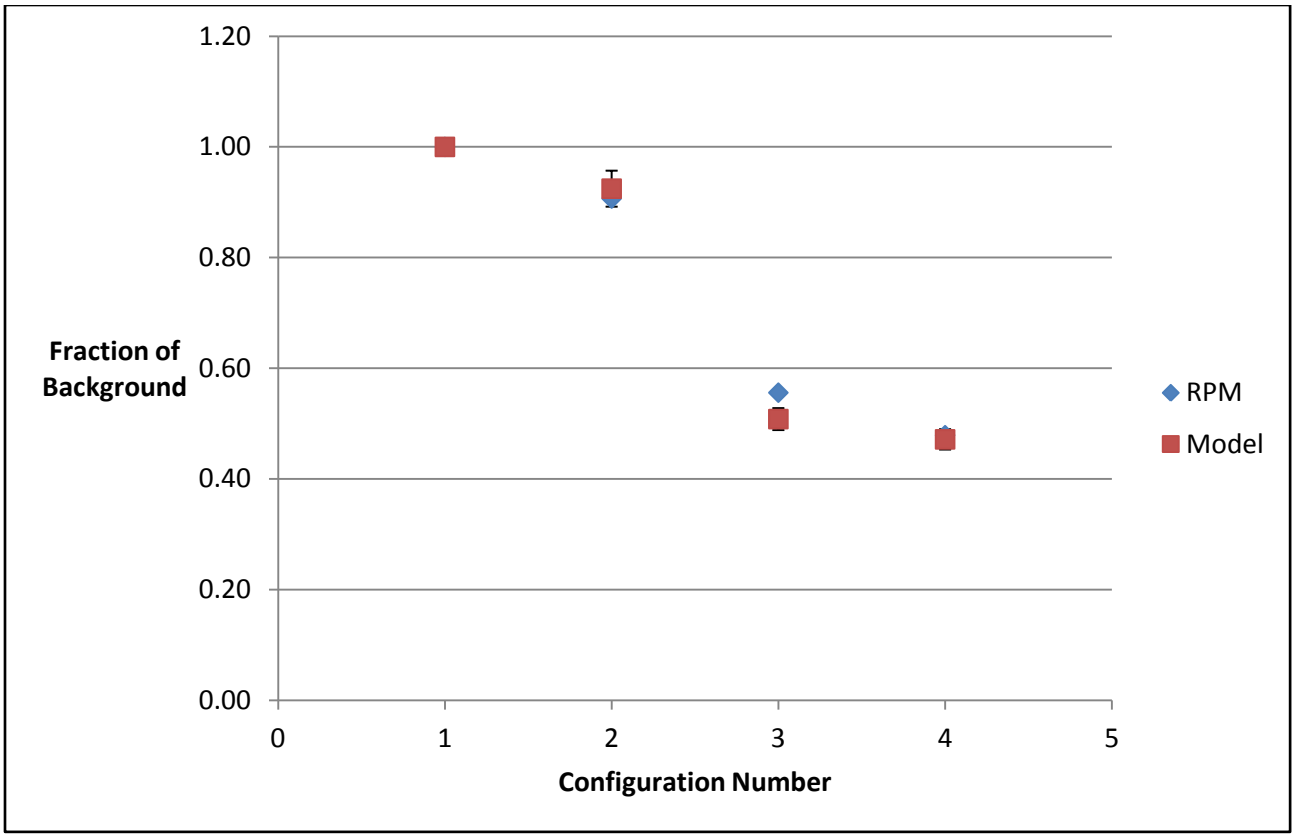

Figure 14. A plot of the fraction of background calculated from slab F RPM and model data.

Table 12. Slab F RPM and model background comparison

	Fraction of Background	
Configuration Number	RPM	Model
1	1	1
2	0.91 ± 0.0004	0.92 ± 0.03
3	0.56 ± 0.0004	0.51 ± 0.02
4	0.48 ± 0.0003	0.47 ± 0.02

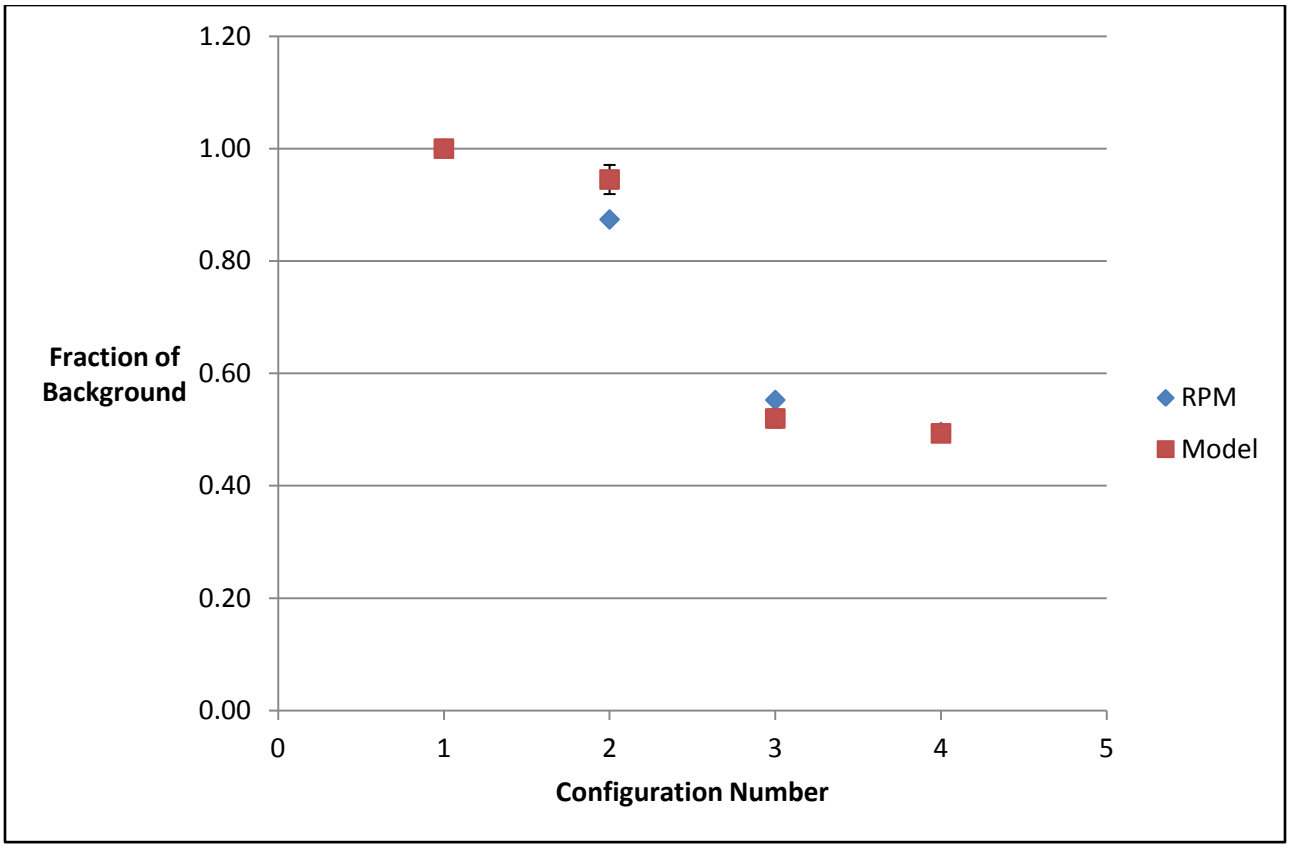

Figure 15. A plot of the fraction of background calculated from slab L RPM and model data.

Table 13. Slab L RPM and model background comparison

	Fraction of Background	
Configuration Number	RPM	Model
1	1	1
2	0.87 ± 0.0004	0.95 ± 0.03
3	0.55 ± 0.0005	0.52 ± 0.02
4	0.50 ± 0.0003	0.49 ± 0.01

6. EXAMPLE PROCEDURE FOR CALCULATIONS

The procedure outlines the course of action required to utilize the developed model in a new location with a different RPM. The same steps used to complete this study can be repeated to determine the influence of a planned installation to remediate high background levels.

1. Obtain daily files from an operating RPM and calculate the average count rate of each detector. Rain events and other external factors that influence RPM background must not be included in the averaged data.

2. Characterize the existing RPM configuration and the planned remediation techniques to aid the formulation of the computer model.[11] Table A.4 and Figures A.4–A.7 in Section A.4 of Appendix A show examples of the required information.

3. Obtain a high-purity germanium spectrum of the asphalt between the RPM pillars.

4. Calculate the specific activity of the asphalt using the ISOCS software.

5. Develop a source card for the computer model based on the isotopic of the asphalt.

6. Create a computer model for both the existing configuration and the configuration with the planned remediation techniques in place.

7. Compare the activity-corrected interaction probabilities from the computer models and calculate the effect of the remediation techniques.

7. CONCLUSIONS

An accurate model of the RPM at the ORNL test bed has been established and is capable of calculating the reduction in background due to remediation techniques to within 10% of measured values. The model can be utilized to determine the effect of remediation techniques before installation so costly mistakes can be avoided. New techniques for background remediation can also be tested with the model to provide justification for field deployment. The ORNL test bed will continue to provide a realistic field environment in a controlled setting for the advancement of RPM technologies. The addition of the model to the existing capabilities of the test bed allows calculations to accompany field data and expand the boundaries of experiments conducted at the test bed.

8. REFERENCES

1. *Vehicle Monitor VM-250AGN Operations & Service Manual*, TSA Systems, Ltd., Doc 5039 Revision A, January 2011.

2. "Multichannel Analyzer Alignment Procedure for TSA Radiation Portal Monitors," Los Alamos National Laboratory, January 26, 2012.

3. "Second Line of Defense Functional Compliance Test Procedure for TSA Radiation Portal Monitors," Los Alamos National Laboratory, SLD-PR-101, Rev. 1, March 2010.

4. J. Livesay et al., *Rain-Induced Increase in Background Radiation Detected by Radiation Portal Monitors*, Oak Ridge National Laboratory, ORNL/TM-2012/229, July 2012.

5. C. M. Ryan, *Determining the Impact of Concrete Roadways on Gamma Ray Background Readings for Radiation Portal Monitoring Systems*, Texas A&M University, May 2011.

6. *ISOCS Calibration Software Technical Reference Manual*, Model S573 V4.2, Canberra Industries, Inc., 2009.

7. F. B. Brown et al., MCNP5-1.51 Release Notes, Los Alamos National Laboratory, LA-UR-09-00384, January 2009.

8. M. B. Fitzmaurice, *Developing a Methodology for Characterizing the Effects of Building Materials' Natural Radiation Background on a Radiation Portal Monitoring System*, Texas A&M University, December 2012.

9. X-5 Monte Carlo Team, MCNP – A General Monte Carlo N-Particle Transport Code, Version 5, Volume I: Overview and Theory, Los Alamos National Laboratory, LA-UR-03-1987, April 24, 2003.

10. R. J. McConn Jr et al., *Compendium of Material Composition Data for Radiation Transport Modeling*, PNNL-15870 Rev. 1, March 4, 2011.

11. T. Guzzardo and N.Rowe, *Procedures for Testing and Documenting Characteristics of MPC&A Installed Radiation Portal Monitors*, Oak Ridge National Laboratory. ORNL/TM-2012/573, December 2012.

APPENDIX A

A.1 Calibration Details

A Cs-137 source was positioned on the yellow circle on each polyvinyl toluene (PVT) detector, and spectra were recorded for the first- and second-stage gain. The first-stage potentiometer (Figure A.1) was adjusted until the local maximum was in channel 40 (±3). The second-stage potentiometer (Figure A.2) was adjusted until the local maximum was in channel 150 (±5).

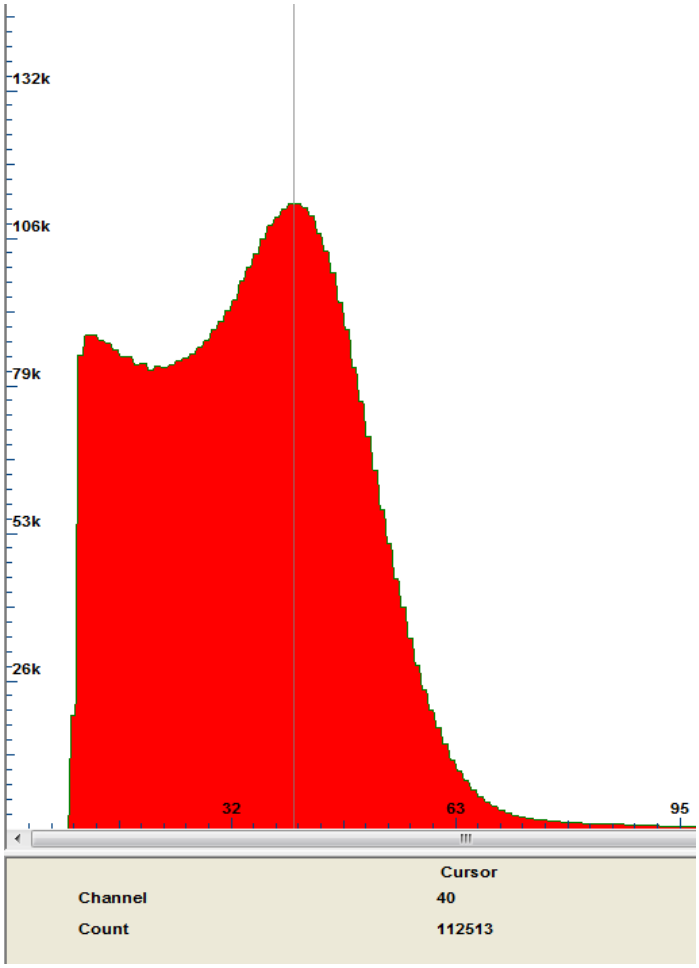

Figure A.1. First-stage gain alignment.

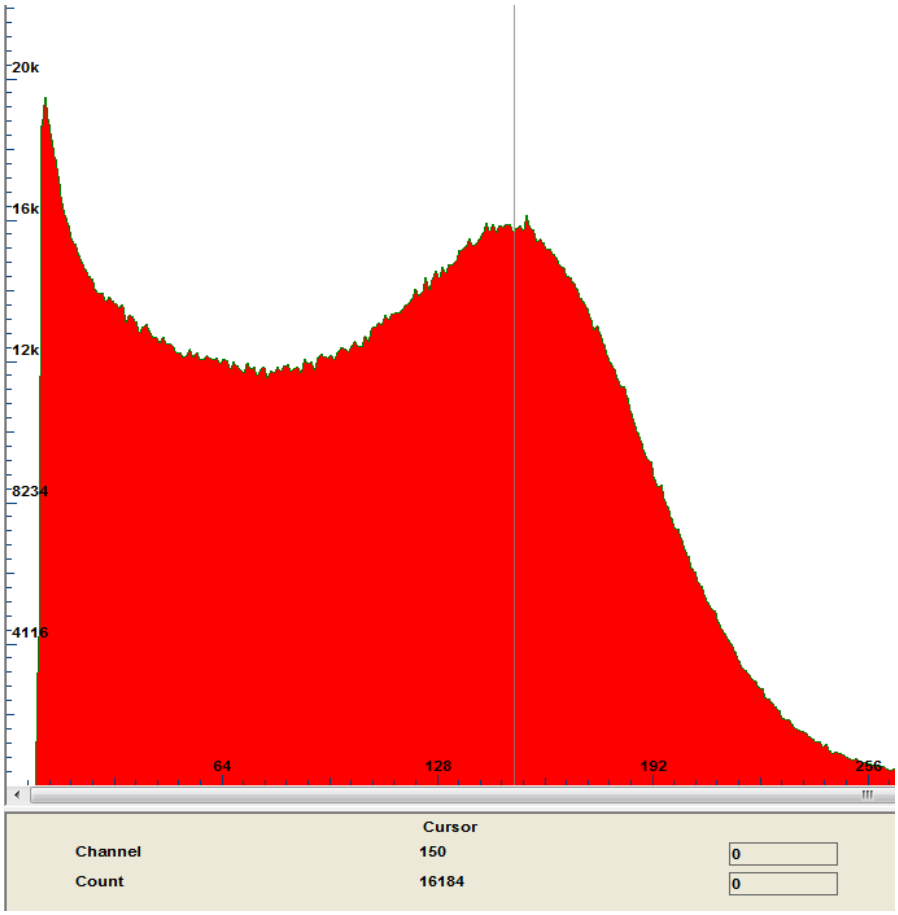

Figure A.2. Second-stage gain alignment.

The efficiency of each detector was calculated by first measuring the background and then measuring a Co-57 source taped to the yellow circle on each PVT slab. Five readings were obtained from each detector and then averaged for use in calculating the detector efficiency (Tables A.1 and A.2). The properties of the Co-57 source used for the measurements are listed in Table A.3.

Table A.1. Background count rates for efficiency calculation

	Trial 1	Trial 2	Trial 3	Trial 4	Trial 5	Average
D1	62	63	61	61	61	62
D2	58	57	58	59	59	58
D3	71	72	73	72	70	72
D4	89	90	89	87	86	88

Table A.2. Co-57 count rates for efficiency calculation

	Trial 1	Trial 2	Trial 3	Trial 4	Trial 5	Average
D1	6054	6046	6074	6066	6050	6058
D2	5898	5893	5896	5897	5891	5895
D3	7624	7611	7619	7605	7590	7610
D4	7798	7786	7757	7768	7772	7776

Table A.3. Co-57 source details

ID Number	Co-57-5711
Initial Activity (μCi/kBq)	93 / 3441
Source Calibration Date	August 1, 2008
Measure Date	March 13, 2013
Decay time (years)	4.61
Co-57 Half-Life (years)	0.74
Current activity (μCi/kBq)	1.24 / 45.80

A.2 Source Terms

Source terms for the MCNP input decks are shown below for concrete slabs G, L, and F in addition to the asphalt. The values listed on the SI card refer to the energy of the gammas emitted from the source. Each gamma energy has a corresponding probability of emission listed on the SP card.

Slab G:

```
SI    L 0.06329 0.09260 0.12907 0.18621 0.23863 0.24200 0.27024
        0.27736 0.29522 0.30009 0.32803 0.33832 0.35193 0.40946
        0.46300 0.58319 0.60931 0.72733 0.76836 0.79495 0.86056
        0.91120 0.93406 0.96477 0.96897 1.12029 1.23811 1.37767
        1.46081 1.76449 2.20421 2.61453
SP    D 0.00656 0.00761 0.00550 0.00655 0.09843 0.01355 0.00787
        0.00516 0.03519 0.00746 0.00671 0.02562 0.06856 0.00436
        0.01000 0.06904 0.08405 0.02335 0.00901 0.00966 0.01014
        0.05865 0.00552 0.01134 0.03592 0.02753 0.01056 0.00729
        0.21047 0.02808 0.00926 0.08102
```

Slab F:

```
SI    L 0.06329 0.09260 0.12907 0.18621 0.23863 0.24200 0.27024
        0.27736 0.29522 0.30009 0.32803 0.33832 0.35193 0.40946
        0.46300 0.58319 0.60931 0.72733 0.76836 0.79495 0.86056
        0.91120 0.93406 0.96477 0.96897 1.12029 1.23811 1.37767
        1.46081 1.76449 2.20421 2.61453
SP    D 0.01800 0.02088 0.00354 0.01128 0.06332 0.02335 0.00506
        0.00332 0.06065 0.00480 0.00431 0.01648 0.11815 0.00281
        0.00643 0.04441 0.14486 0.01502 0.01552 0.00621 0.00652
        0.03773 0.00952 0.00730 0.02310 0.04745 0.01819 0.01257
        0.13276 0.04839 0.01596 0.05211
```

Slab L:

```
SI    L 0.06329 0.09260 0.12907 0.18621 0.23863 0.24200 0.27024
        0.27736 0.29522 0.30009 0.32803 0.33832 0.35193 0.40946
        0.46300 0.58319 0.60931 0.72733 0.76836 0.79495 0.86056
        0.91120 0.93406 0.96477 0.96897 1.12029 1.23811 1.37767
        1.46081 1.76449 2.20421 2.61453
SP    D 0.01208 0.01402 0.00377 0.00764 0.06745 0.01581 0.00539
        0.00354 0.04106 0.00511 0.00460 0.01756 0.07999 0.00299
        0.00685 0.04731 0.09807 0.01600 0.01051 0.00662 0.00695
        0.04019 0.00645 0.00777 0.02461 0.03212 0.01232 0.00851
        0.29564 0.03276 0.01081 0.05552
```

Asphalt:

SI L 0.12907 0.18621 0.23863 0.24200 0.27024 0.27736 0.29522 0.30009
0.32803 0.33832 0.35193 0.40946 0.46300 0.58319 0.60931 0.66166
0.72733 0.76836 0.79495 0.86056 0.91120 0.93406 0.96477 0.96897
1.12029 1.23811 1.37767 1.46081 1.76449 2.20421 2.61453

SP D 0.00272 0.00687 0.04868 0.01421 0.00389 0.00255 0.03691 0.00369
0.00332 0.01267 0.07190 0.00216 0.00495 0.03414 0.08816 0.04462
0.01155 0.00945 0.00478 0.00501 0.02901 0.00579 0.00561 0.01776
0.02888 0.01107 0.00765 0.40279 0.02945 0.00971 0.04007

A.3 RPM Data Selection

Each RPM configuration was measured for multiple days before data was selected for averaging. Data was used from time periods free of rain events and other irregular detector responses. The black boxes in Figure A.3 show the time periods of data used from the sample set.

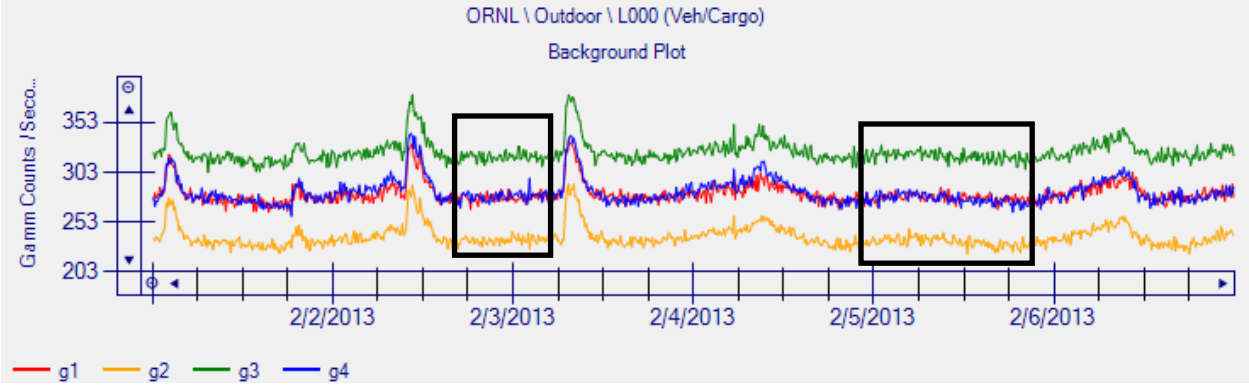

Figure A.3. Example selection of background data.

A.4 RPM Characterization

Table A.4 shows what parameters need to be measured in the field to update the RPM model. It can be used to document RPM characteristics with the aid of Figures A.4–A.7.

Table A.4. Existing RPM characterization information

Manufacturer:		
Model number:		
Collimator dimensions (cm):		
Number of pillars:		
Pillar elevation from asphalt (cm):		
Distance between pillar doors (cm):		
Pillar-to-pillar offset (cm):	Horizontal:	
	Vertical:	
Asphalt aggregate:		
Notes:		

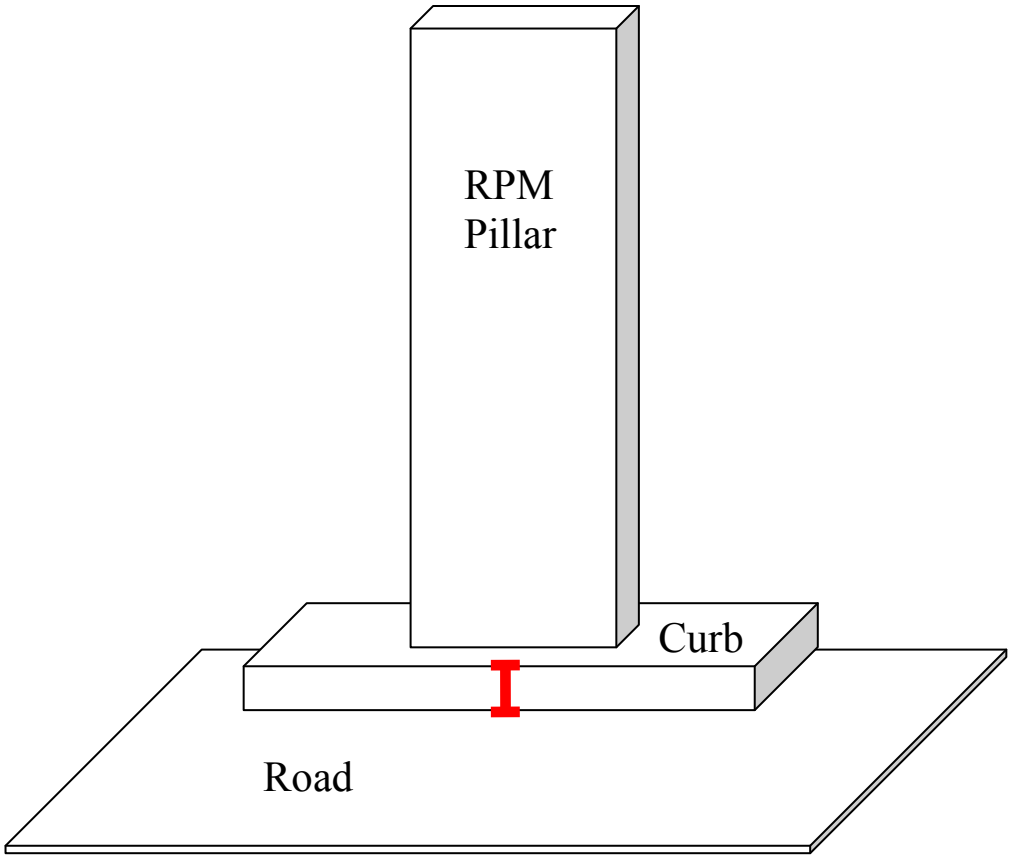

Figure A.4. Pillar elevation from surface.

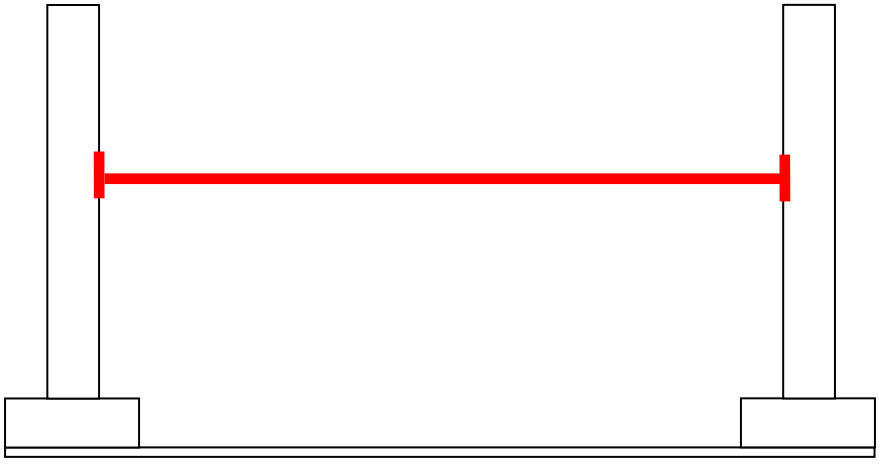

Figure A.5. Distance between pillar doors.

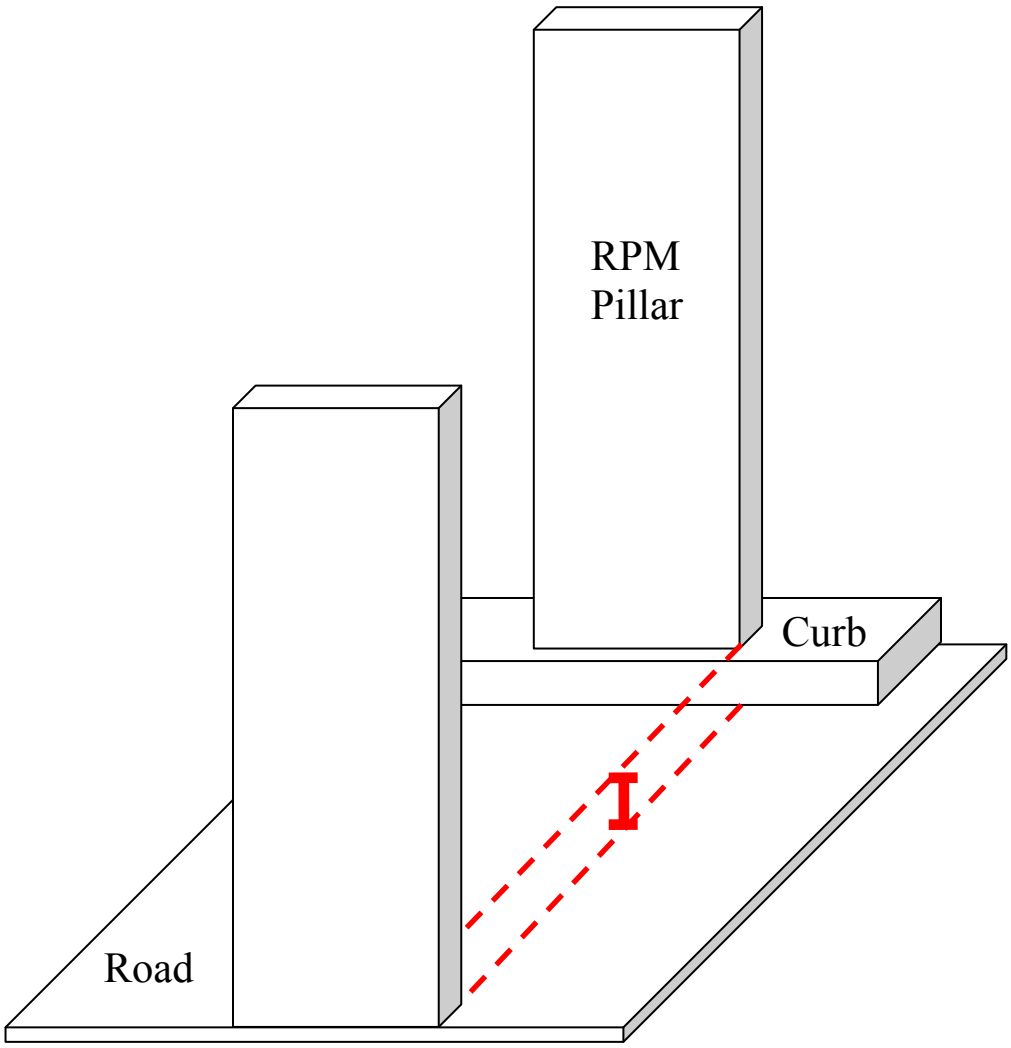

Figure A.6. Vertical pillar-to-pillar offset.

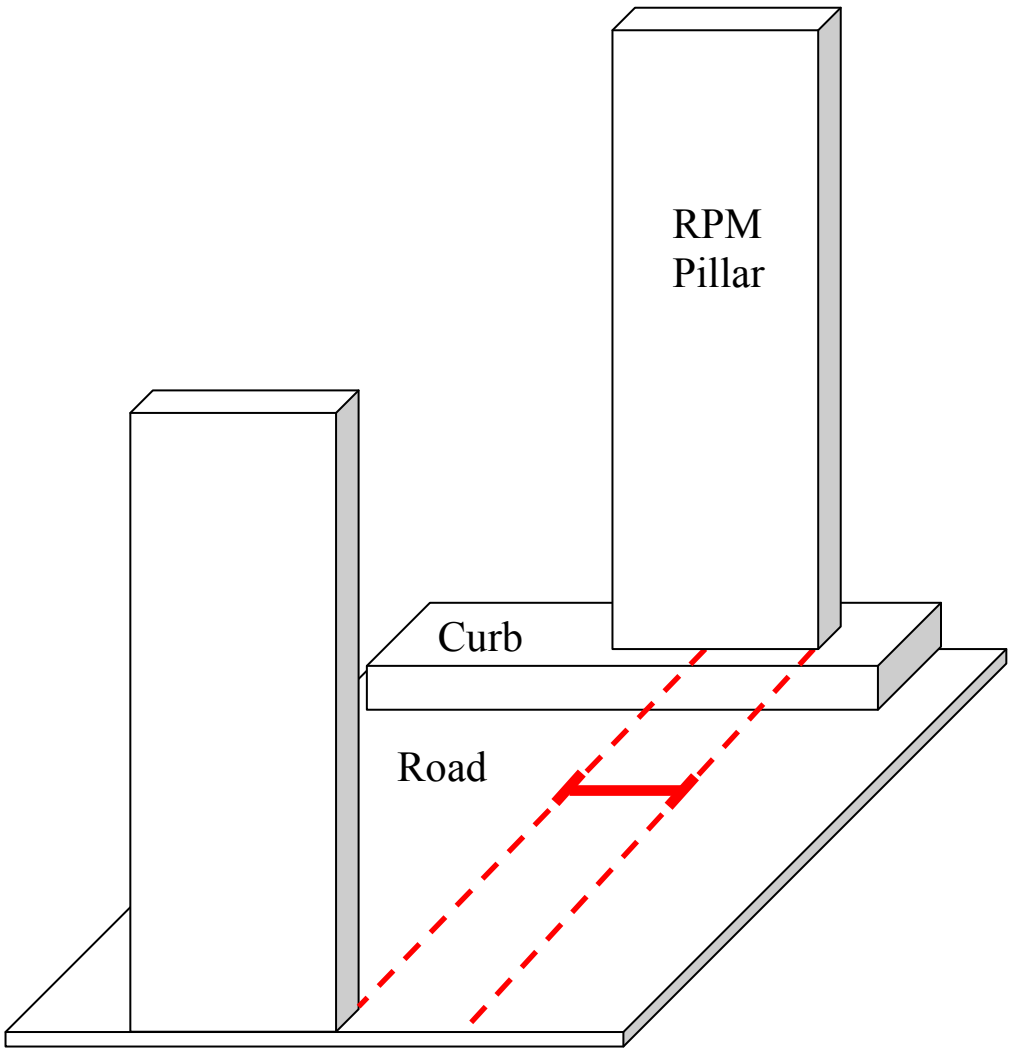

Figure A.7. Horizontal pillar-to-pillar offset.